Vacancy formation mechanism and synergy with doping in NiS_2-based electrocatalyst for benzyl alcohol oxidation and hydrogen evolution

Fang Li [a], *Haili Lin* [a], *Huiqin Yu* [a], *Pengfei Du* [a], *Yang Wang* [b,*], *Jing Cao* [a,*]

[a] Key Laboratory of Green and Precise Synthetic Chemistry and Applications, Ministry of Education; College of Chemistry and Materials Science, Huaibei Normal University, Huaibei, Anhui 235000, P. R. China

[b] Department of Applied Biology and Chemical Technology and Research Institute for Smart Energy, The Hong Kong Polytechnic University, Kowloon, Hong Kong SAR, P. R. China

Content

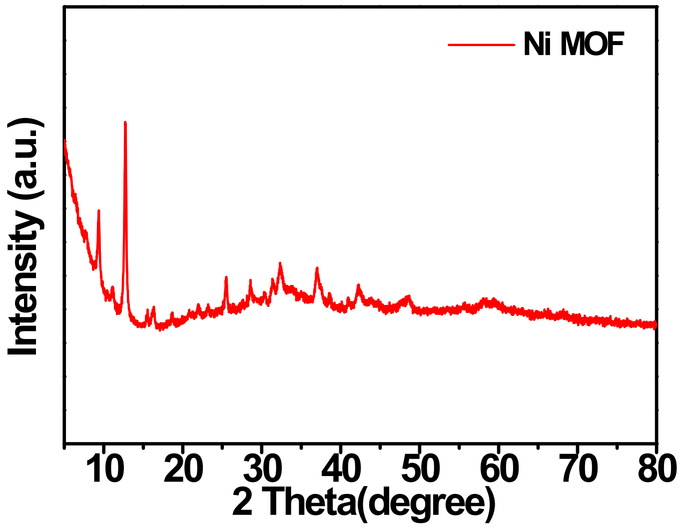

Fig. S1. XRD pattern of Ni MOF

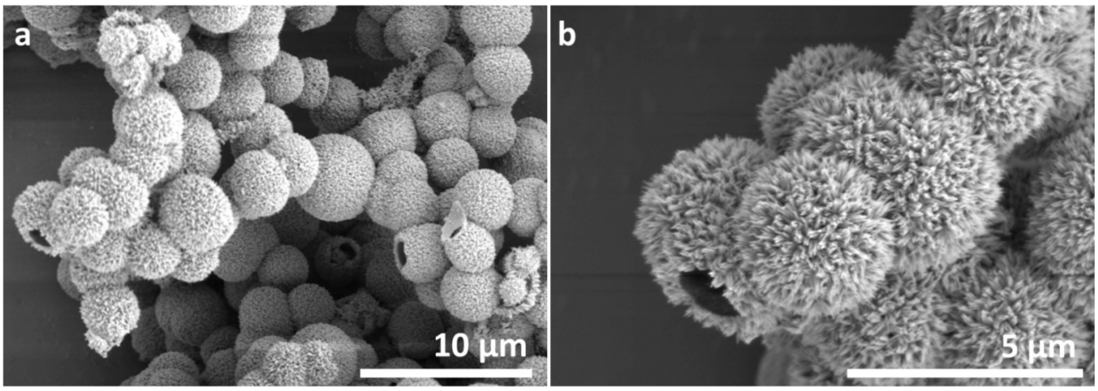

Fig. S2. the SEM of the MOF

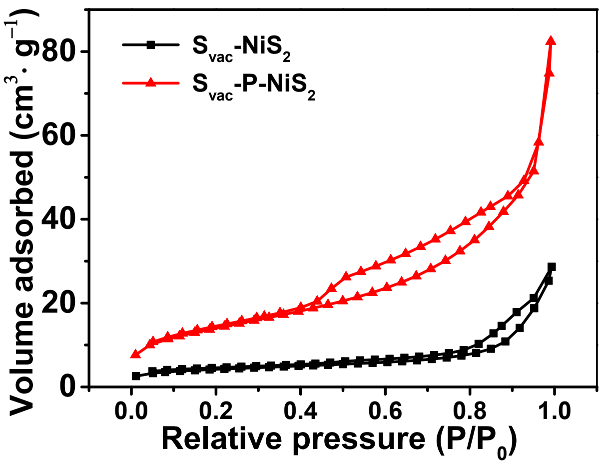

Fig. S3. Nitrogen adsorption-desorption isotherm of the S_{vac}-P-NiS_2 and S_{vac}-NiS_2

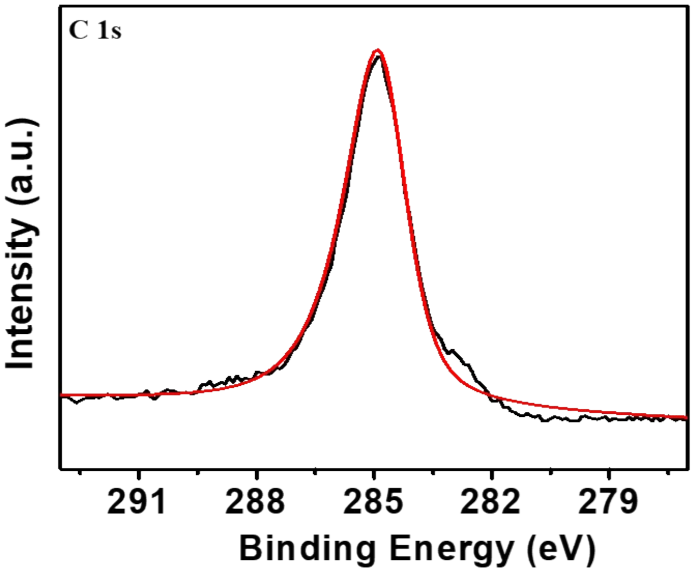

Fig. S4. the C 1s XPS of the S_{vac}-P-NiS_2

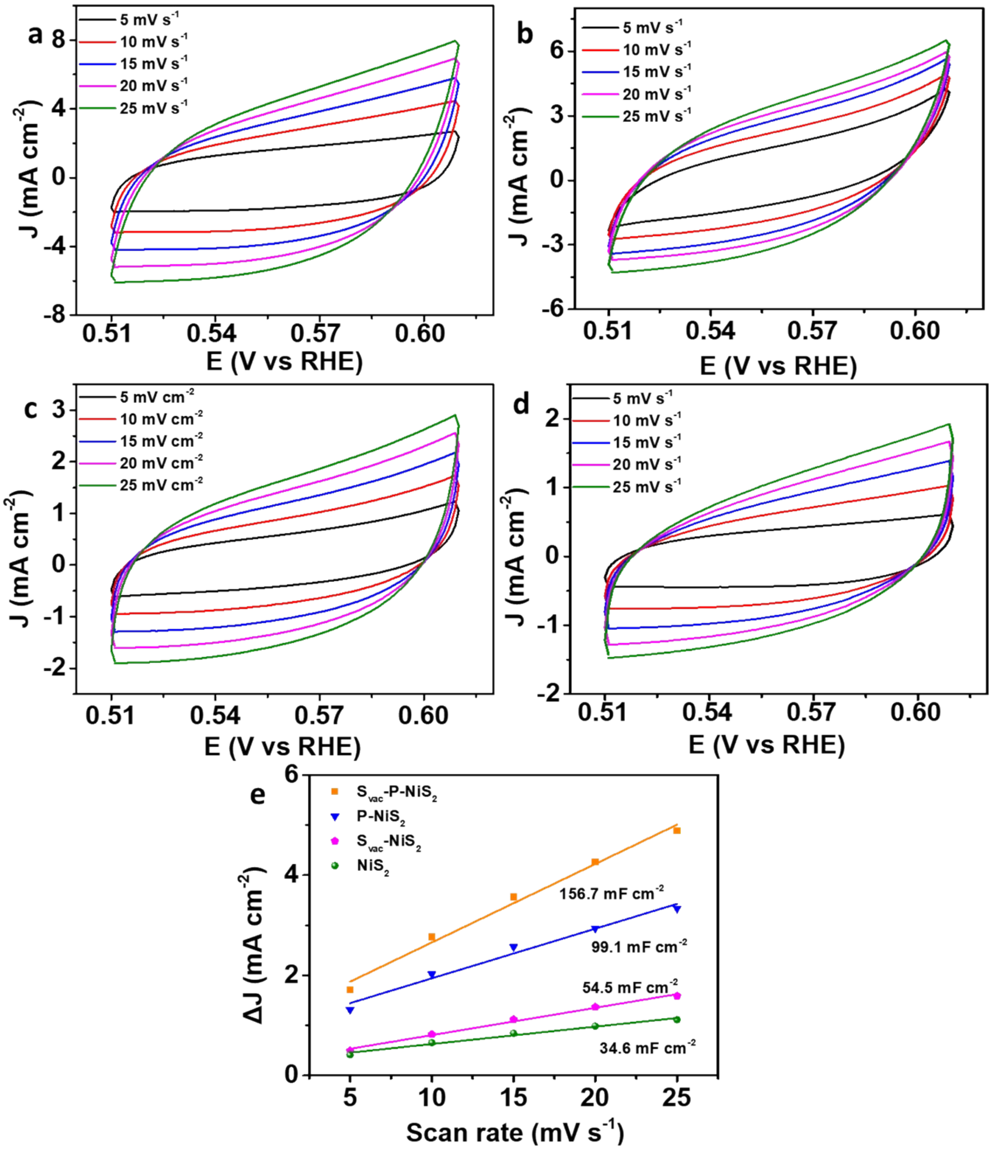

Fig. S5. The C_{dl} of S_{vac}-P-NiS_2, P-NiS_2, S_{vac}-NiS_2, and NiS_2 for the BA oxidation.

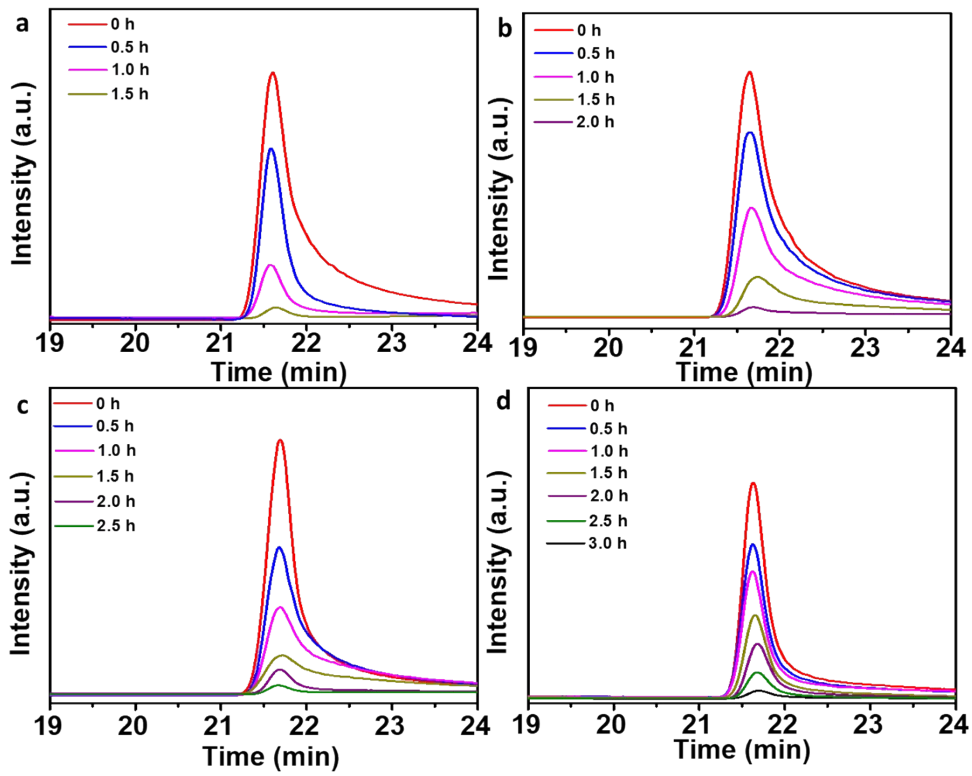

Fig. S6. The HPLC results of benzyl alcohol for (a) S_{vac}-P-NiS_2, (b) P-NiS_2, (c) S_{vac}-NiS_2, (d) NiS_2.

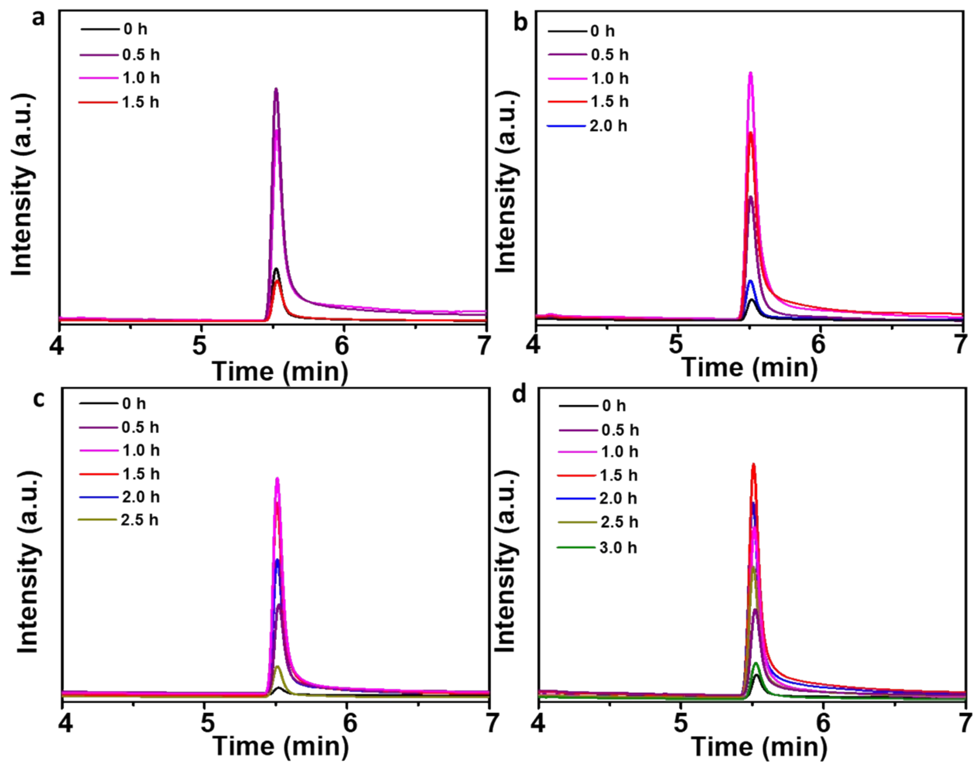

Fig. S7. The HPLC results of benzaldehyde for (a) S_{vac}-P-NiS_2, (b) P-NiS_2, (c) S_{vac}-NiS_2, (d) NiS_2.

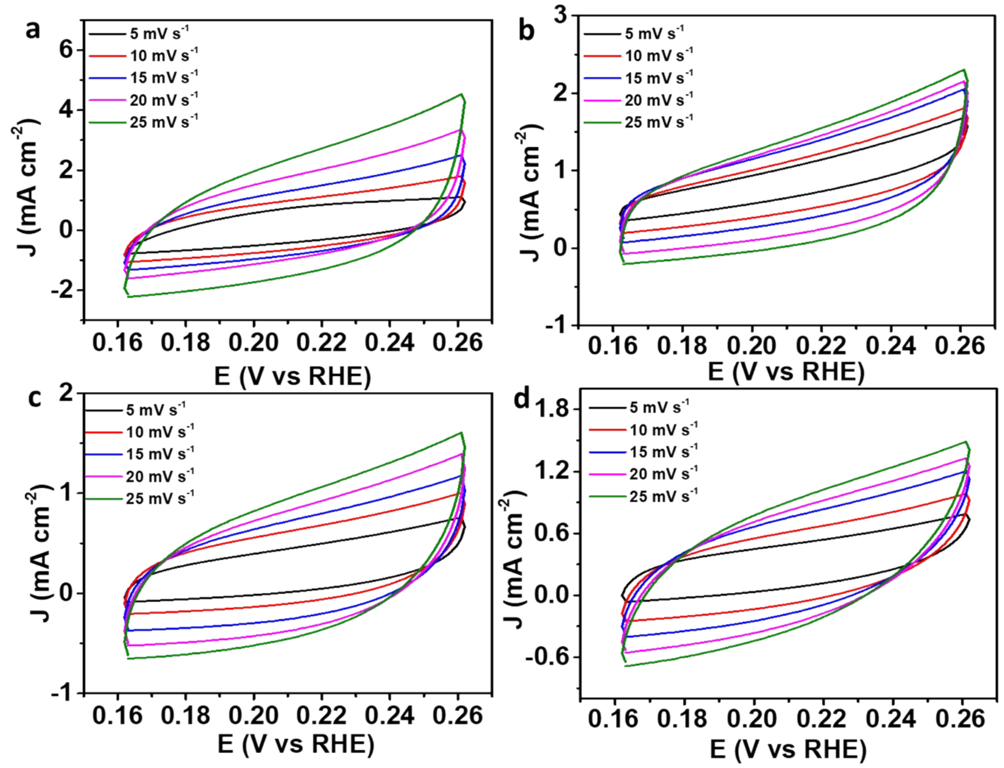

Fig. S8. CV curves measured at different scan rates (5, 10, 15, 20, 25 mV s^{-1}). (a) S_{vac}-P-NiS_2, (b) P-NiS_2, (c) $S_{vac}NiS_2$, (d) NiS_2. For the HER

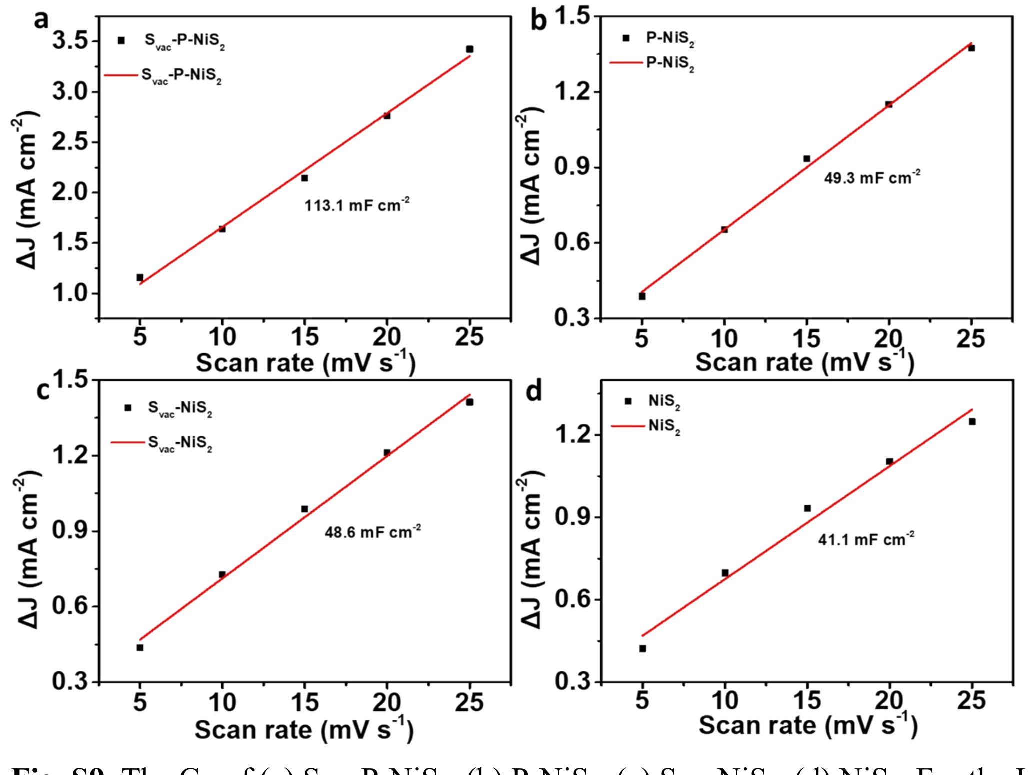

Fig. S9. The C_{dl} of (a) S_{vac}-P-NiS_2, (b) P-NiS_2, (c) S_{vac}-NiS_2, (d) NiS_2. For the HER

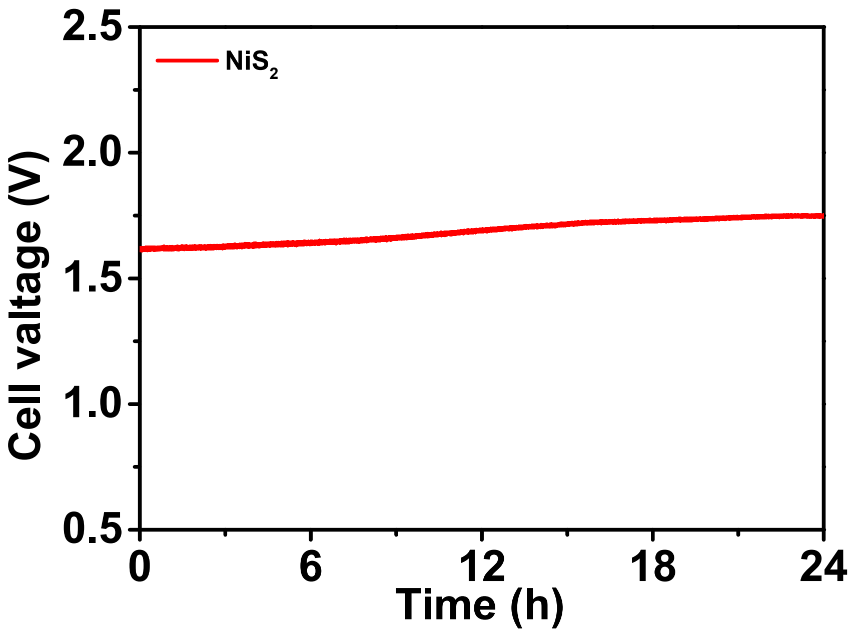

Fig. S10 the stability of the pristine NiS_2

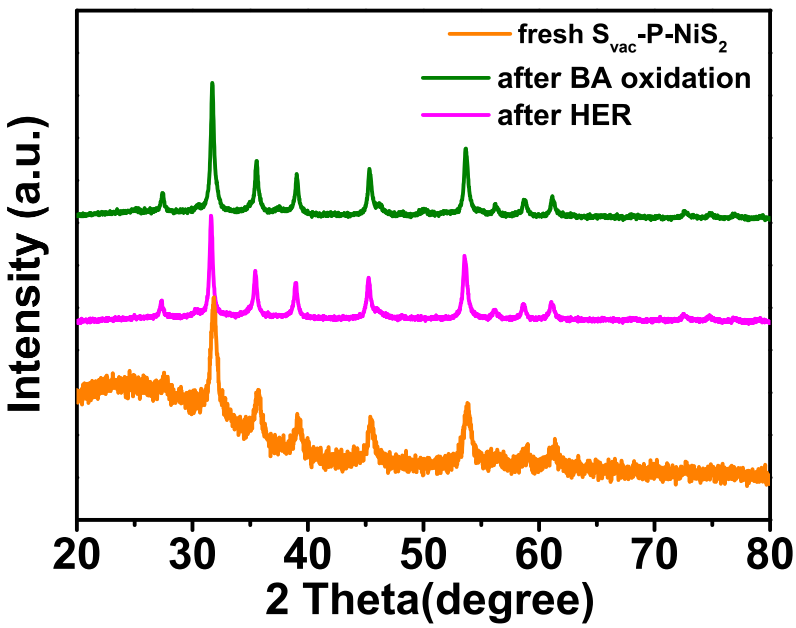

Fig. S11 The XRD after long term BA oxidation and HER for the S_{vac}-P-NiS_2

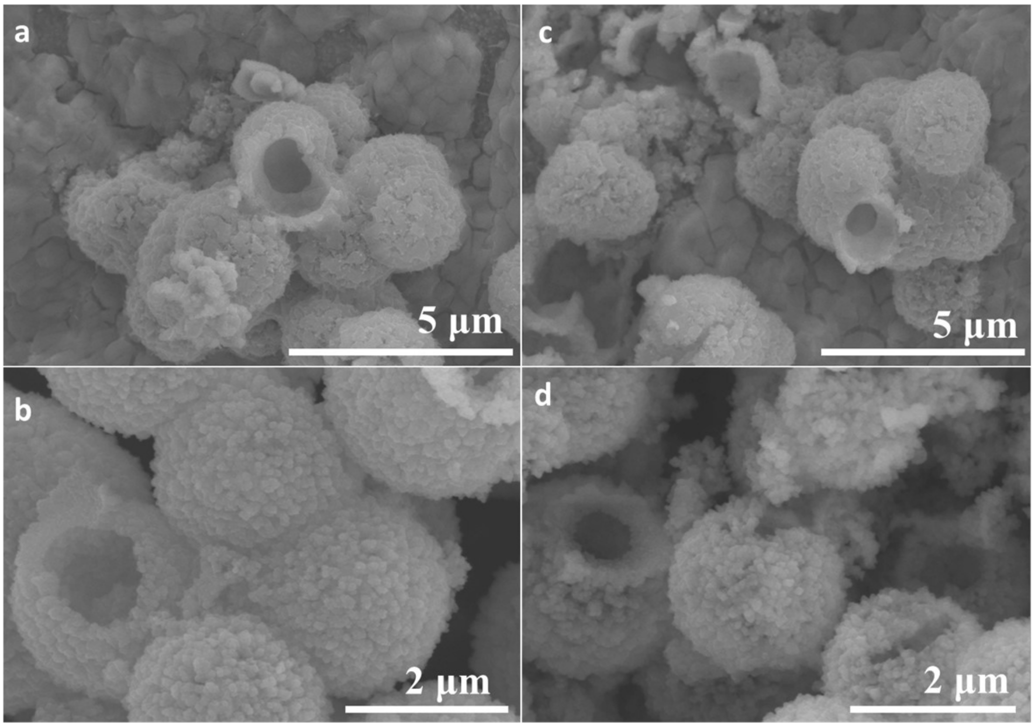

Fig. S12. the SEM of the after long term BA oxidation (a and b) and HER (c and d)

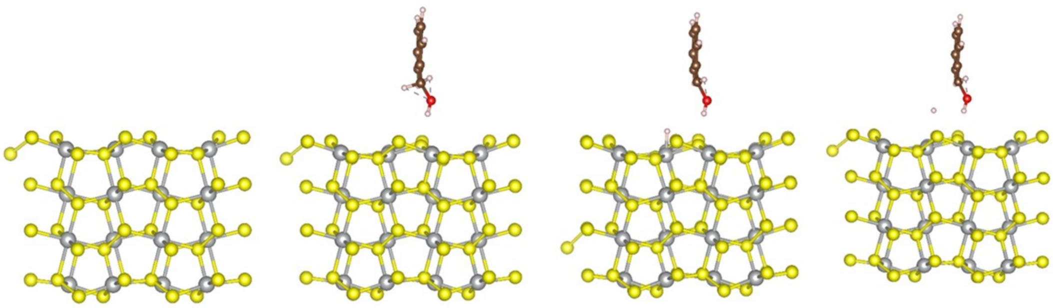

(a) The optimized structure of the NiS_2

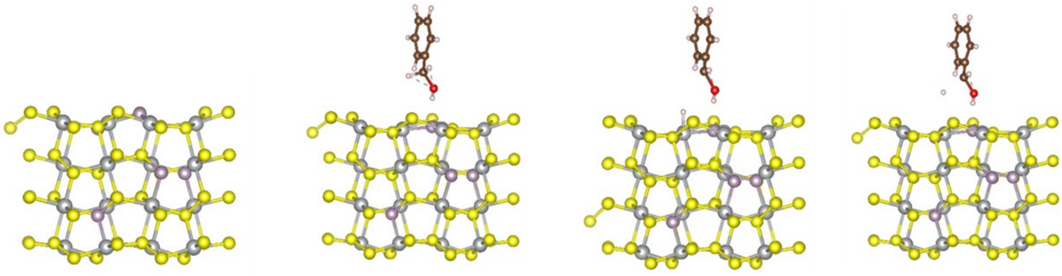

(b) The optimized structure of the P-NiS_2

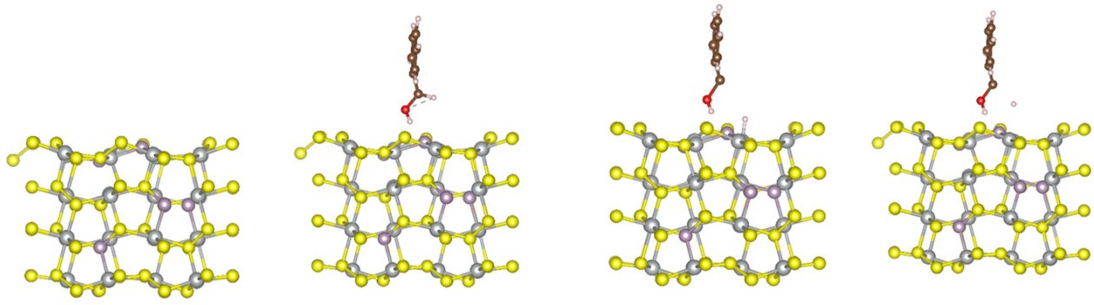

(c) The optimized structure of the S_{vac}-P-NiS_2

Fig. S13. the optimized structure

Calculation method

All the DFT calculations were conducted based on the Vienna Ab-inito Simulation Package (VASP). The exchange-correlation effects were described by the Perdew-Burke-Ernzerhof (PBE) functional within the generalized gradient approximation (GGA) method. The core-valence interactions were accounted by the projected augmented wave (PAW) method. The energy cutoff for plane wave expansions was set to 480 eV, and the 3×3×1 Monkhorst-Pack grid k-points were selected to sample the

Brillouin zone integration. The vacuum space is adopted 15 Å above the surfaces to avoid periodic interactions. The structural optimization was completed for energy and force convergence set at 1.0×10^{-4} eV and 0.02 eV $Å^{-1}$, respectively.

The Gibbs free energy change (ΔG) of each step is calculated using the formula: ΔG = ΔE + ΔZPE - TΔS, where ΔE is the electronic energy difference directly obtained from DFT calculations, ΔZPE is the zero point energy difference, T is the room temperature (298.15 K) and ΔS is the entropy change. ZPE could be obtained after frequency calculation by: ZPE = $\frac{1}{2}\sum hvi$

And the TΔS values are calculated according to the vibrational frequencies:

$$T\Delta S = k_BT\left[\sum_k ln(\frac{1}{1-e^{-hv/k_BT}}) + \sum_k \frac{hv}{k_BT}\frac{1}{(e^{hv/k_BT}-1)} + 1\right]$$

Table S1 the comparison of the BA oxidation

Catalysts	Electrolyte (1 M KOH with BA)	Product	E (V vs. RHE)	Current density (mA cm^{-2})	Ref.
S_{vac}-P-NiS_2	50 mM	Benzoic acid	1.21	50	This work
CC@NiO/Ni_3S_2	0.2 M	Benzoic acid	1.365	50	1
Hp-Ni	10 mM	Benzoic acid	1.35	10	2
NC@$CuCo_2N_x$/CF	15 mM	Benzoic acid	1.25	10	3
Mo-Ni	10 mM	Benzoic acid	1.345	15	4
N–Mo–Ni/NF	0.1 M	Benzaldehyde	1.338	100	5
$Co_{0.83}Ni_{0.17}$/AC	10 mM	Benzoic acid	1.28	10	6
h-$Ni(OH)_2$	40 mM	Benzoic acid	1.43	20	7
Fe/Co(oxide)	15 mM	Benzoic acid	1.438	10	8
$NiCo_2O_4$/NF	50 mM	Benzoic acid	1.46	100	9
MnFeCoNiCu	0.1 M	Benzoic acid	1.57	100	10
Ni_2P	50 mM	Benzoic acid	1.32	30	11
Ni_xCo1-HCF HN	0.1 M	Benzoic acid	1.33	10	12

1 R.C. Li, P.Y. Kuang, L.X Wang, H.L. Tang, J.G. Yu, Engineering 2D NiO/Ni_3S_2 heterointerface electrocatalyst for highly efficient hydrogen production coupled with benzyl alcohol oxidation, *Chem Eng J.,* 2022, **431**, 134137.

2 B. You, X. Liu, X. Liu, Y.J. Sun, Efficient H_2 evolution coupled with oxidative refining of alcohols via a hierarchically porous nickel bifunctional electrocatalyst, *ACS Catal.,* 2017, **7** (7), 4564–4570.

3 J. Zheng, X.L. Chen, X. Zhong, S.Q. Li, T.Z. Liu, G.L Zhuang, X.N. Li, S.W. Deng, D.H. Mei, J.G. Wang, Hierarchical porous NC@CuCo nitride nanosheet networks: highly efficient bifunctional electrocatalyst foroverall water splitting and selective electrooxidation of benzyl alcohol, *Adv. Mater.,* 2017, 1704169.

4 X. Liu, X. Cui, M. Chen, R. Xiong, J. Sun and B. Geng, Ultrastable and efficient H_2 production via membrane-free hybrid water electrolysis over a bifunctional catalyst of hierarchical Mo-Ni alloy nanoparticles, *J. Mater. Chem. A.,* 2019, **7**, 16501–16507.

5 J. Wan, X. Mu, Y. Jin, J.K. Zhu, Y.C. Xiong, T.Y. Li, R. Li, Nitrogen-doped nickel-molybdenum oxide as a highly efficient electrocatalyst for benzyl alcohol Oxidation, *Green Chem.,* 2022, **24**, 4870–4876.

6 G.Q. Liu, X. Zhang, C.J. Zhao, Q.Z. Xiong, W.B. Gong, G.Z. Wang, Y.X. Zhang, H.M. Zhang, H.J. Zhao, Correction: electrocatalytic oxidation of benzyl alcohol for simultaneously promoting H_2 evolution by a $Co_{0.83}Ni_{0.17}$/activated carbon electrocatalyst, *New. J. Chem.,* 2019, **43**, 7881.

7 X.L. Chen, X. Zhong, B.W. Yuan, S.Q. Li, Y.B. Gu, Q.Q. Zhang, G.L. Zhuang, X.N. Li, S.W. Deng, J.W. Wang, Defect engineering of nickel hydroxide nanosheets by ostwald ripening for enhanced selective electrocatalytic alcohol oxidation, *Green Chem.,* 2019, **21**, 578-588.

8 Y.Y. Huang, R. Yang, G. Anandhababu, J.F. Xie, J.Q. Lv, X.T. Zhao, X.Y. Wang, M.X. Wu, Q.H. Li, Y.B. Wang, Cobalt/Iron (oxides) heterostructures for efficient oxygen evolution and benzyl qlcohol oxidation reactions, *ACS Energy Lett.,* 2018, **3**, 1854–1860.

9 M. Xu, J. Geng, H. Xu, S. Zhang, H. Zhang, In situ construction of $NiCo_2O_4$ nanosheets on nickel foam for efficient electrocatalytic oxidation of benzyl alcohol, *Inorg Chem Front.,* 2023, **10** (7), 2053–2059.

10 B. Singh, R. Kumar, A. Draksharapu, Multimetallic prussian blue analogue nanoparticles for oxygen evolution reaction and efficient benzyl alcohol oxidation, *ACS Applied Nano Mater.,* 2024, **7** (13), 15763–15771.

11 F. Li, C. Liu, H. Lin, Y. Sun, H.Q. Yu, X.M. Jia, S. Xue, J. Cao, S.F. Chen, High activity of bifunctional Ni_2P electrocatalyst for benzyl alcohol oxidation coupled with hydrogen evolution, *J. Colloid Interface Sci.,* 2023, **640**, 329–337.

12 C. Lv, L. Chen, J. Bai, H. Ruo, Y. Pan, S. Xu, J. Chen, D. Zhang, C. Guo, Ni-Co hexacyanoferrate hollow nanoprism with CN vacancy for electrocatalytic benzyl alcohol oxidation. *Chem Commun.,* 2024, **60** (46), 5952–5955.

Table S2 EIS fitting results for BA oxidaion.

	S_{vac}-P-NiS_2	P-NiS_2	S_{vac}-NiS_2	NiS_2
Rs	2.541	2.856	2.978	2.739
Rct	10.29	13.99	16.49	29.78
CPE-T	0.00026369	0.00017668	0.00019744	0.00012944
CPE-P	0.73101	0.7932	0.7267	0.83402
χ^2	0.071193	0.079766	0.062145	0.058712

Table S3 EIS fitting results for HER.

	S_{vac}-P-NiS_2	P-NiS_2	S_{vac}-NiS_2	NiS_2
Rs	2.752	2.86	2.752	2.755
Rct	11.78	11.72	11.78	30.93
CPE-T	0.00016389	0.0003318	0.00016389	0.00012495
CPE-P	0.7943	0.70396	0.7943	0.83894
χ^2	0..048664	0.076587	0.048664	0.059591